ACS OMEGA

http://pubs.acs.org/journal/acsodf

Article

Immobilization of Cubic Silver Plasmonic Nanoparticles on TiO_2 Nanotubes, Reducing the Coffee Ring Effect in Surface-Enhanced Raman Spectroscopy Applications

Robert Ambroziak, Jan Krajczewski, Marcin Pisarek,* and Andrzej Kudelski

Cite This: *ACS Omega* 2020, 5, 13963−13972

Read Online

ACCESS | Metrics & More | Article Recommendations

ABSTRACT: Surface-enhanced Raman spectroscopy (SERS) substrates prepared by immobilizing silver cubic nanoparticles (Ag CNPs) on titanium dioxide nanotubes (TiO_2 NTs) were used for investigations of the "coffee ring" (CR) effect and its impact on spatial reproducibility of measured Raman signals in comparison with flat surfaces (Ti and Si) where the CR effect is usually significant. The immobilization of nanoparticles from drops, which is a very simple technique, usually does not permit a homogeneous distribution of deposited NPs because there is significant accumulation of the material at the boundary of the drying area. Our proposed SERS substrates effectively reduced the CR effect through the use of well-ordered nanostructures where a smaller number of Ag CNPs were transferred to the boundary region. It was not only the surface morphology that was important but also the physicochemical properties of TiO_2 NTs, such as wettability. The wettability of the prepared samples was determined by measuring the static water contact angle (WCA), and the chemical composition near the boundary of the drying area was studied using Auger electron spectroscopy. The morphology of the substrates obtained was characterized using scanning electron microscopy. Our studies showed that reducing the coffee ring effect increased the spatial reproducibility of the measured SERS signal in the area of the deposited CNPs. Therefore, the platforms obtained may be very useful in commercial SERS applications.

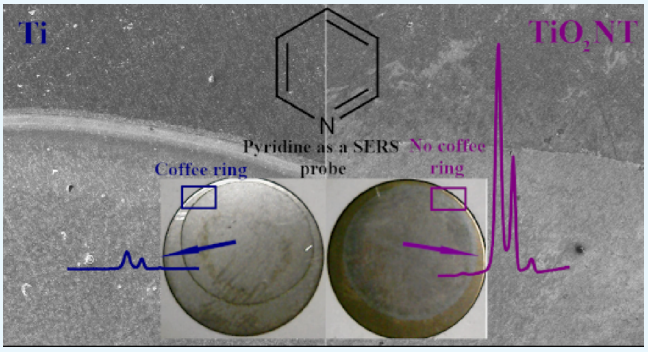

INTRODUCTION

When nanostructures formed from metals with a negative real and small positive imaginary dielectric constant (for example, silver or gold nanoparticles) interact with electromagnetic radiation, an oscillation of the surface conduction electrons is induced, which leads to an increase in the intensity of the electric field near the illuminated nanostructures. The enhancement of the intensity of the electric field generated leads to a significant increase in the efficiency of a number of optical processes for molecules located in the space where the intensity of the electric field was increased. For example, the generated field enhancement leads to amplification of the efficiency of the generation of Raman spectra in an effect known as surface-enhanced Raman scattering (SERS). In some cases, the SERS enhancement factor generated is very large, permitting observation of Raman spectra of even a single molecule,[1−3] and SERS is therefore one of the most sensitive analytical tools available. The numerous applications of SERS mean that the preparation of efficient and reproducible SERS substrates is a rapidly developing field of applied science and technology. Many methods for the synthesis of materials for SERS measurements have been developed, for example, printing,[4−8] sputtering,[9−11] or blocking nanoparticles[12−15] on the substrate. In the case of blocking, the linkers that connect the nanoparticles to the substrate are usually used.[16,17] Experimentally, the easiest method used for depositing films of plasmonic nanoparticles is to deposit a suspension of such nanoparticles on the substrate and evaporate the solvent. Unfortunately, this very simple technique usually does not make it possible to obtain homogeneous SERS substrates because, due to the "coffee ring" (CR) effect, there is significant accumulation of the plasmonic material at the boundary of the drying area (although, for some SERS materials, the appearance of the CR effect is desirable; see below). The CR effect occurs when a solution containing solutes dries on the substrate[18,19] and manifests as a characteristic line surrounding the place where the drop was

Received: March 26, 2020
Accepted: May 14, 2020
Published: June 3, 2020

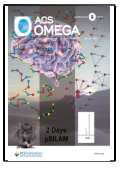

https://dx.doi.org/10.1021/acsomega.0c01356
ACS Omega 2020, 5, 13963−13972

previously located. Examples of this effect are the stains from wine or coffee formed on various surfaces. The CR effect appears because of the flow inside the drop as it dries.[19] Near the surface, flow is directed away from the center of the drop, transferring substances to its edge. Drying stops these substances near the edge of the drop. This effect has been carefully tested on various substrates, and the results obtained make it possible, for example, to design new SERS substrates where this effect may be desirable.[20−22] SERS substrates manufactured by applying nanoparticles in suspension and letting them dry make it possible to obtain aggregates at the boundary of the deposited drop (due to the CR effect) that have a highly ordered structure. The substrates thus obtained exhibit a high SERS enhancement factor (achievable over a relatively small area). Unfortunately, the coffee ring effect is usually unwanted in SERS measurements.[23−25] A common reason for avoiding it in SERS substrates is to ensure repeatability of measurements. Decreasing the CR effect should increase the even distribution of plasmonic nanoparticles on the surface, so that regardless of where SERS measurements are taken, similar enhancement factors are obtained over the entire surface. Many groups have attempted to decrease the CR effect during the preparation of SERS substrates. One method is to use magnetic−plasmonic composites and carry out drying of the substrate when it is covered by the magnetic−plasmonic nanomaterial in a strong magnetic field.[26] Other attempts to decrease the CR effect involve controlling the wettability of the substrate[25] and drying a drop that is hanging.[23,24]

A number of factors affect whether the coffee ring effect is observed,[18,27] one of them being the wettability of the substrate. Superhydrophobic substrates prevent the CR effect[28,29] because the contact line of the droplets with the surface is small and the capillary flow from the center of the drop is blocked. In the case of hydrophobic substrates, the effect is larger, but still, the smaller contact line does not permit a significant CR effect.[30−32] However, when the substrate is hydrophilic or superhydrophilic, the coffee ring effect causes significant accumulation of the substance at the edge of the drop.[28−32] This is because the drop dries faster near the contact line than away from it. There is a flow of liquid along with substances from the center of the droplet to its edge. There, after drying, the substances remain immobilized. The next factor affecting the CR effect is the morphology of the surface on which the droplet is located.[32,33] The presence of nanopillars on the surface causes a disturbance of flow inside the droplet, which in turn reduces mass transport to the edge of the sample, thereby reducing the CR effect.[27,32] On the other hand, when the surface is porous, the liquid from the drop penetrates it until the solution completely fills the available space.[33,34] This causes an additional retention of nanoparticles on the surface due to capillary forces that direct the substance toward the substrate.[33] The use of porous substrates or nanopillars on the surface leads to increased substance retention on the substrate away from the contact line, which reduces the CR effect.

In this work, we tested one substrate for the simple preparation of an efficient material for SERS measurements for which one can expect that the CR effect should be significantly reduced, namely, a titanium substrate covered with a layer of titanium(IV) oxide nanotubes (TiO_2 NT). We found that, due to its specific morphology and physicochemical properties such as wettability, it was actually possible to use this substrate for the formation of films of silver nanoparticles by depositing a suspension of Ag nanoparticles and evaporating the solvent; the CR effect for films formed of Ag nanoparticles was significantly smaller than for films formed on Ti substrates before nanostructuring. It is known from the literature and in our previously studies that the diameter of TiO_2 nanotubes changed with the applied voltage of anodic oxidation. Thus, a linear relationship between these parameters is generally observed. It can also be seen that, as the anodization voltage increases, the distance between the tubes also increases. From 3D visualization, it was found that the TiO_2 nanotubes are initially separated at the top and connected at the bottom.[35,36] Moreover, the material obtained in such a case displayed a low background in the SERS measurements, which makes it very useful as a substrate for such measurements.

RESULTS AND DISCUSSION

Contact Angle Measurements. To determine the wettability of the titanium (Ti), flat titanium oxide (TiO_2 flat), and titanium nanotube (TiO_2 NT) substrates, contact-angle measurements were carried out. The contact angle was determined for samples without a Ag CNP deposit. The results are summarized in Table 1 and are consistent with the literature data.[36−39] The substrate of titanium oxide nanotubes with a contact angle of 4° has superhydrophilic properties. It seems that the surface structure, in terms of crystallinity and morphology, is the main factor affecting the hydrophilicity of the annealed nanotubes at 450 °C.[36] Annealing at 450 °C also changes the structure of the TiO_2 oxide from the amorphous to crystalline phase, anatase. Thus, the presented results suggest that the coffee ring effect should occur on flat titanium oxide, pure Ti, and Si where the water contact angles (WCA) were 87°, 68°, and 60°, respectively.[28−32] However, it should be noted that contact-angle measurement makes it possible to some extent to determine whether the CR effect will be formed only for smooth samples.

Table 1. Contact Angle of the Titanium (Ti) Substrate, Flat Titanium (IV) Oxide (TiO_2 Flat), and Titanium(IV) Oxide Nanotubes (TiO_2 NT)

sample	contact angle
Si	60°
Ti	68°
TiO_2 flat	87°
TiO_2 NT	4°

SEM Measurements. To determine the width of the layer of nanoparticles deposited due to the CR effect at the boundary of the drying area, SEM measurements were made for all three substrates after spotting the cubic silver nanoparticles (Ag CNPs). Nanoparticles have previously been used to study the coffee ring effect.[20−25] For example, Yunker et al.[40] describe the effect of the anisotropicity of nanoparticles on the CR effect, but their work focuses on elliptical-shaped nanostructures. It has been noticed that these types of nanoparticles do not produce coffee rings as effectively as spherical ones do. In our work, we used cubic nanoparticles with an edge length of 45 ± 2 nm to significantly increase the achievable SERS enhancement,[41] and one can assume that experiments with spherical nanostructures would give slightly different results.

https://dx.doi.org/10.1021/acsomega.0c01356
ACS Omega 2020, 5, 13963−13972

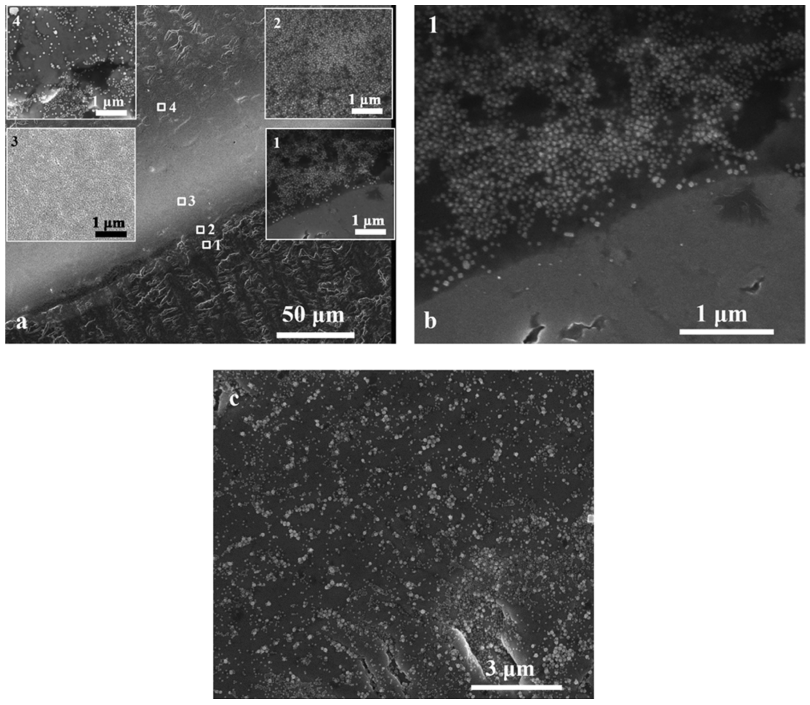

Figure 1. (a) SEM image of a border of a dried drop on titanium. The width of the layer of densely packed nanoparticles (resulting from the coffee ring effect) is 56 μm. (b) Border of the CR. (c) SEM image from the middle of the drop.

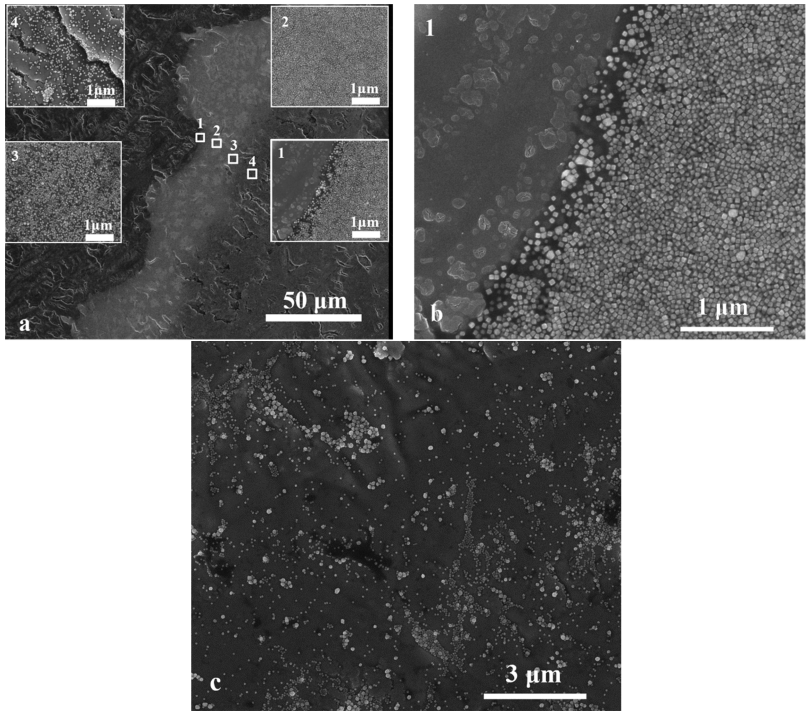

Figure 2. (a) SEM image of the border of a dried drop on flat titanium oxide. The width of the layer of densely packed nanoparticles (resulting from the coffee ring effect) is 44 μm. (b) Border of CR. (c) SEM image from the middle of the drop.

The SEM study was performed after spotting and drying the suspension of nanoparticles on the substrates for which the contact angles were measured. In this way, it was possible to show the morphology of each substrate. Figure 1a shows the results of the SEM measurements for the pure titanium substrate. The measured width of the area of densely packed nanoparticles was 56 μm. In inset 1, Figure 1b, it can be seen that, apart from the boundary set by the aggregate of nanoparticles, no nanostructures can be seen. Then, in insets 2 and 3, it can be seen that the packing density increases as it moves deeper into the dried drop. This may be due to the flow that, over time, spans more nanoparticles, although some of the solvent would dry out earlier, leaving fewer nanoparticles packed along the edge of the CR. At inset 4, it can be seen that the packing is much smaller inside the drop. Figure 1c shows the inside of the drop on titanium after it has dried. The

https://dx.doi.org/10.1021/acsomega.0c01356
ACS Omega 2020, 5, 13963−13972

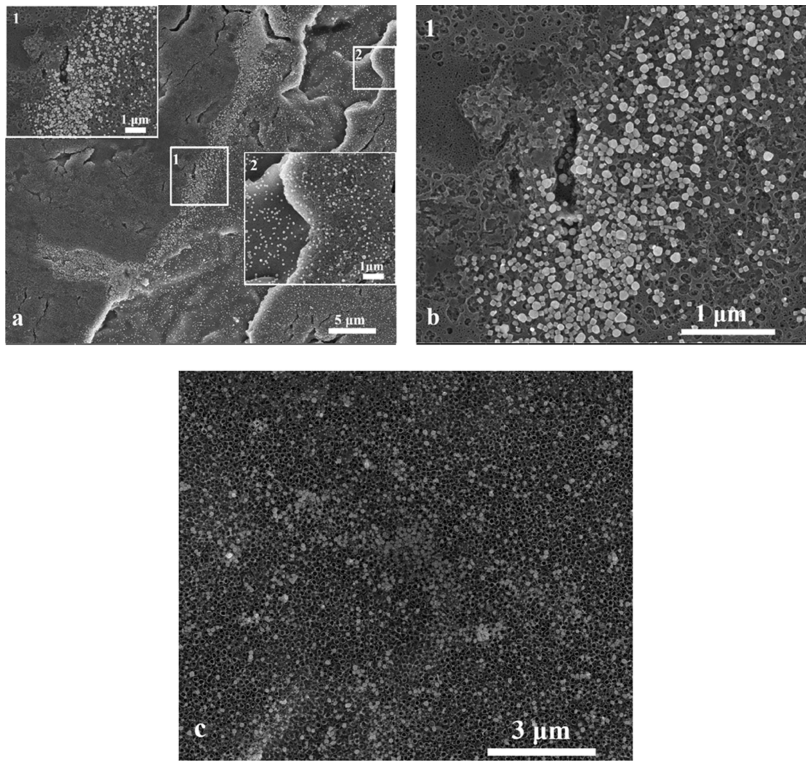

Figure 3. (a) SEM image of the border of a dried drop on titanium oxide nanotubes. The width of the layer of densely packed nanoparticles due to the coffee ring effect is ca. 2 μm . (b) Border of CR. (c) SEM image from the middle of the drop.

substrate is not evenly covered, and a certain number of agglomerates are visible (and hence, the achievable SERS enhancement should strongly depend on the place at which the SERS spectrum is measured). SERS measurements at the places where agglomerates occur should give much greater enhancement factors than at the places where there are only single nanoparticles. In addition, the number of nanoparticles can vary significantly at different places in the sample, which can additionally affect the value of the SERS signal.

Similar results were obtained for a layer of nanoparticles deposited on a flat titanium oxide substrate (see Figure 2a). For this sample, the width of the layer of densely packed nanoparticles created by the CR effect was 44 μm. Again, no nanoparticles are visible just behind the edge of the droplet (Figure 2b). In this case, the packing of Ag CNPs is large from the beginning of the covered area (insets 1 and 2 in Figure 2). This may be due to pinning of the contact line on the hydrophobic substrate.[19] The drop border on this type of substrate does not shift as the drop dries. Fewer and fewer nanoparticles remain that could migrate due to the CR effect (insets 3 and 4 in Figure 2), and finally, inside the droplets, we get only loosely packed nanoparticles. In Figure 2c again, there is a relatively small surface coverage in the middle of the area covered by nanoparticles. The surface coverage is even smaller than that for the layer produced on the titanium substrate (see Figure 1c). The ratio of the number of agglomerates to the number of separated nanoparticles also seems to be larger than for the substrate shown in Figure 1c. Near the drop edge (Figure 2a inset 4), the number of nanoparticles on the surface is much higher than inside the sample (see Figure 2c). This may explain why there are far fewer nanoparticles inside the droplet.

In the case of the substrate made of titanium oxide nanotubes with an average pore diameter of ∼110 nm, wall thickness of ∼20 nm, and height of ∼800 nm[36,42] (see Figure 3a), significantly different results were obtained. The Ag CNPs after deposition are mainly located on top of the nanotubes and between them. Therefore, it was possible to obtain an almost completely covered surface of TiO_2 NTs by Ag nanoparticles. The border (a layer of more densely packed nanoparticles) itself is very narrow (only ca. 2 μm) and consists of loosely packed nanoparticles (see Figure 3b). Except for the inner drop, Ag CNPs are also not visible. In this case, the packing density of nanoparticles inside the drop (Figure 3, inset 2) is not so much smaller than in the region of accumulation due to the CR effect. The number of aggregates in relation to separate nanoparticles visible in Figure 3c is much smaller than in the other samples. In addition, the number of nanoparticles in the area outside the CR effect accumulation region is higher than in the substrates with TiO_2 flat (see Figure 2c) and Ti (see Figure 1c). The amount of Ag CNPs near the CR enrichment region (see Figure 3a, insert 2) is similar to the amount of nanoparticles inside the sample (see Figure 3c). Careful analysis of the SEM microscopic images revealed that the largest amount of nanoparticles accumulated on the border was observed for TiO_2 flat then for Ti and the smallest amount for TiO_2 NTs. Visual data was confirmed by SEM image analysis where it was shown that the number of nanoparticles in a 1 μm wide strip of the surface across area of nanoparticle accumulation (from the beginning to the end of the CR area, perpendicular to the line of the CR ring) varies from 25.5×10^3 for TiO_2 flat through 14.1×10^3 for Ti to 0.2×10^3 for TiO_2 NTs. This result clearly indicates reduction of the CR effect depending on the surface morphology and physicochemical properties of the prepared substrates.

https://dx.doi.org/10.1021/acsomega.0c01356
ACS Omega 2020, 5, 13963−13972

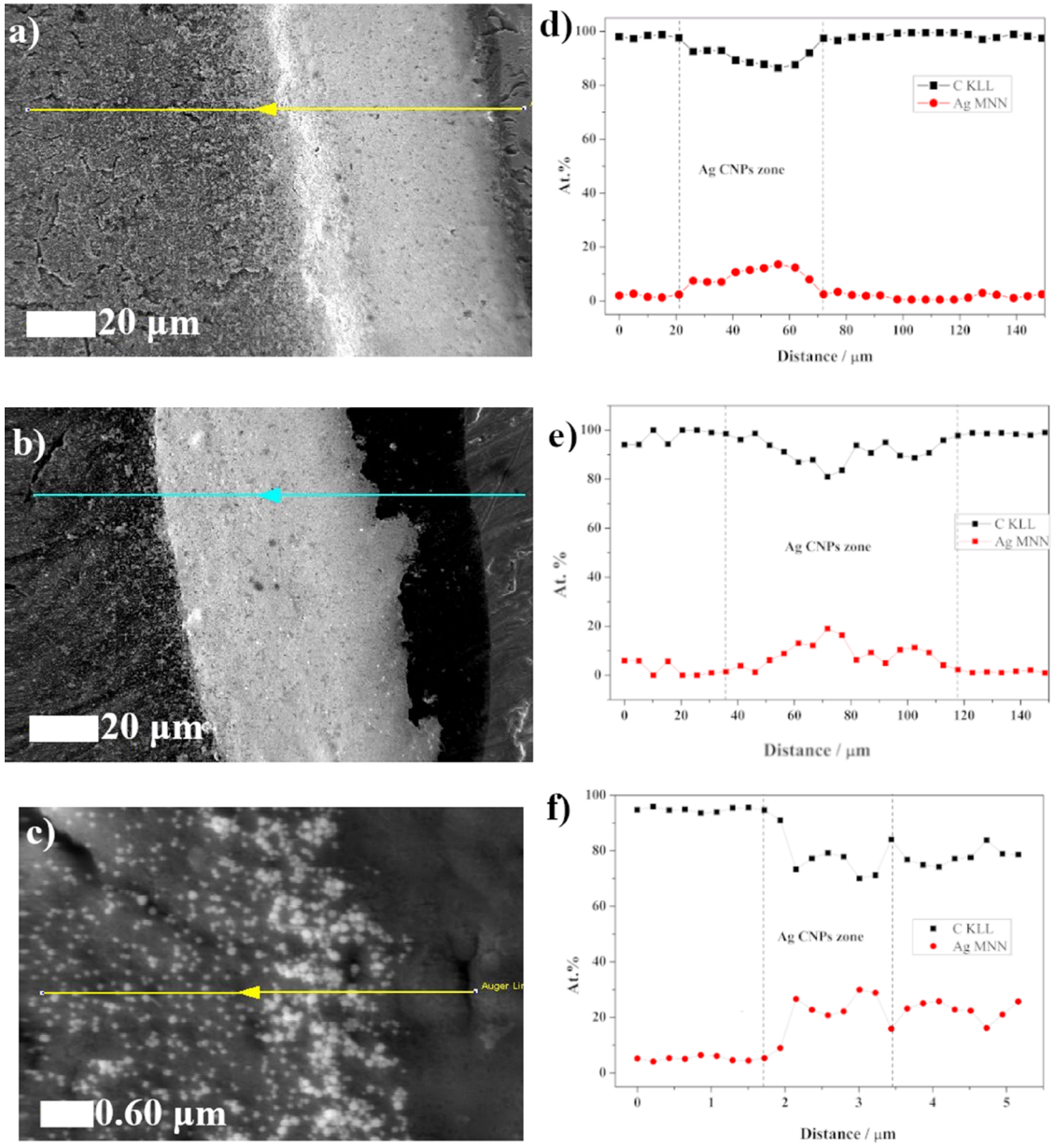

Figure 4. SEM images with the AES profile line: (a) Ti, (b) TiO_2 flat, and (c) TiO_2 NT. Distribution of carbon (black) and silver (red) for (d) Ti, (e) TiO_2 flat, and (f) TiO_2 NT over the AES profile line. Widths of the agglomerate area resulting from the coffee ring effect calculated from SEM measurements: (a) Ti: 56 μm, (b) TiO_2 flat: 63 μm, and (c) TiO_2: 1.5 μm. Widths of the agglomerate area resulting from the coffee ring effect calculated by AES: (d) Ti: 43 μm, (e) TiO_2 flat: 82 μm, and (d) TiO_2 NT: 1.7 μm.

All these observations show that the layers of silver nanoparticles obtained on titanium oxide nanotubes have a significantly more suitable structure for reproducibility of SERS measurements than that of the layers formed on the other analyzed substrates.

Auger Electron Spectroscopy (AES) Measurements. The AES measurements were correlated with the SEM observations. The widths of the "border layers" obtained were similar to those in the previous SEM measurements at 43, 82, and 1.7 microns for Ti (Figure 4a), TiO_2 flat (Figure 4b), and TiO_2 NT (Figure 4c), respectively. An AES line scan analysis over 150 μm was made for Ti (Figure 4d) and TiO_2 flat (Figure 4e) samples, while for the TiO_2 NT (Figure 4f) sample, the measurement width was 5.5 μm. The line scan indicates that the amount of carbon near the "CR region" was relatively high. This was due to the presence of anti-aggregation polyvinylpyrrolidone (PVP), which was used during the synthesis of the Ag CNPs. PVP prevents agglomeration of nanoparticles and stabilizes their growth during synthesis.[43] After cleaning the nanoparticles, it remained attached to the surface of the Ag CNPs. Therefore, the area of densely packed nanoparticles formed a compact layer with a high content of carbon. In this region, we can also observe an increase in the AES signal from silver, as shown in Figure 4d,e. This result clearly indicates the presence of a CR effect for pure Ti and TiO_2 flat. A similar result was obtained for the sample with nanotubes, though the effect was observed on a much smaller scale. AES linear analysis showed the absence of a clear boundary between the droplet and nanoporous substrate as seen in the change in the silver and carbon signals (Figure 4f).

https://dx.doi.org/10.1021/acsomega.0c01356
ACS Omega 2020, 5, 13963−13972

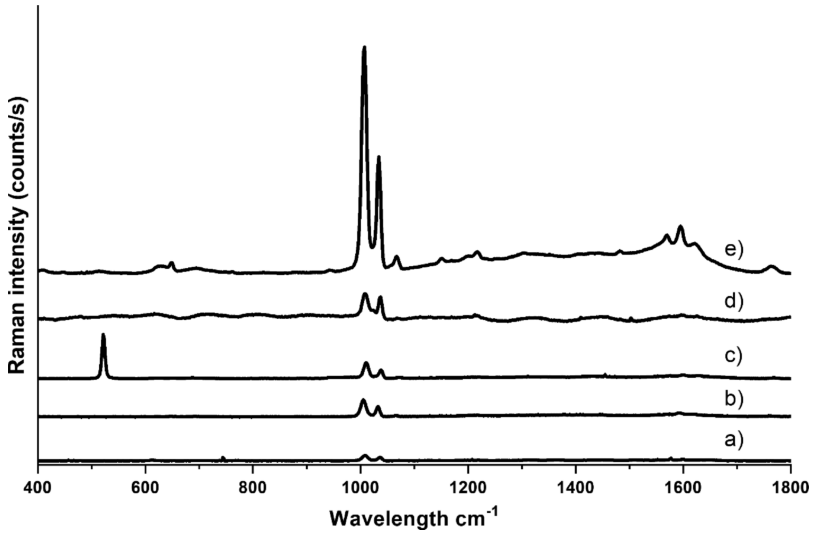

Figure 5. SERS spectra collected from the center of the substrate of silver cubic nanoparticles on (a) TiO_2 flat, (b) titanium, (c) silicon, and (e) TiO_2 nanotubes. (d) Spectrum collected from the rough silver electrode. In spectrum c the band at 520 cm^{-1} is due to silicon substrate.

Taking into account the linear distribution of silver, it was possible to determine the broadness of the coffee ring. Measured with AES, this was 43, 82, and 1.7 μm for Ti, TiO_2 flat, and TiO_2 NT, respectively. It should be noted that the measurements were not carried out exactly perpendicular to the CR line, which slightly disturbs the measurement. In the case of Ti and TiO_2 flat samples, the percentage of silver decreased drastically in relation to the CR on the inside of the drop. For the TiO_2 NT sample, this decrease was insignificant. This result confirms the even distribution of nanoparticles on the nanoporous substrate.

Raman Measurements. Figure 5 shows the SERS spectra of pyridine measured using various substrates. Each spectrum presented in this figure was made by averaging 400 spectra collected from different places within the 60 × 60 μm area of the substrate. For each substrate, the volume of solution of cubic nanoparticles dropped was the same. Only the substrate of electro-roughened silver (Figure 5d) did not contain cubic nanoparticles. Characteristic peaks from pyridine at 1004 and 1034 cm^{-1} are visible in all the spectra. For the TiO_2 NT substrate (Figure 5e), a band at 1064 cm^{-1} is also visible.[44] In the other spectra, it is not visible due to the low spectra intensities.

In the spectral range of 1500−1700 cm^{-1} in the spectra collected using the TiO_2 NT substrate, a characteristic carbon background[45] is visible. The spectrum intensity obtained on the TiO_2 NT is higher than that for the rest of the substrates. The background of the spectrum obtained on the TiO_2 NT outside the spectral region of 1500−1700 cm^{-1} is negligible. Therefore, the use of PVP seems to be a good solution in SERS studies because this polymer gives relatively weak spectra, which was also observed by other researchers.[46,47] Of course, the presence of PVP on the Ag surface can interfere with "SERS analysis of traces of organic compounds", but this is a general problem in this type of measurement. The synthesis of cubic nanoparticles is not possible without the use of any surfactant that would not generate any SERS spectrum. The SERS spectrum of the silver cubic nanoparticles on silicon (see Figure 5c) has the appearance of a spectrum when using a substrate other than titanium. It can be seen that the shape and intensity of the spectrum is not strongly dependent on the type of flat surface. In spectrum c in Figure 5 the band at 520 cm^{-1} is due to silicon substrate. Showing the pyridine spectrum on the rough silver electrode (see Figure 5d) was intended to point out the intensity of the pyridine spectrum on a generally known material. As can be seen, the intensity of this spectrum is similar to that of the spectra obtained on the flat substrates and many times smaller than that obtained with AgCNPs@TiO_2 NT.

SERS Activity of the Materials Obtained and Reproducibility of the SERS Measurements. To compare the SERS enhancement factors generated by various materials and estimate the spatial reproducibility of the achievable SERS enhancement factors, for each substrate, 400 spectra were collected at various places on the square surface of a size of 60 μm × 60 μm. For all spectra, the accumulation time was 1 s. Measurements were taken on the center of the sample (away from the area covered by nanoparticles accumulated due to the CR effect). All spectra were taken for pyridine as the SERS sampler. We took the intensity of the pyridine band at 1004 cm^{-1} as the intensity of the measured spectra. Figure 6 shows the logarithms of the intensity of this pyridine band recorded for each of the series of 400 measurements for each analyzed

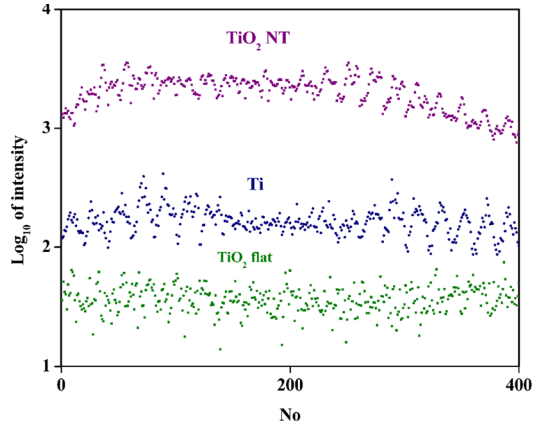

Figure 6. Logarithmic plot of the intensity of the pyridine band at 1004 cm^{-1} recorded in each of the series of 400 measurements of samples TiO_2 NT (violet), Ti (blue), and TiO_2 flat (green).

https://dx.doi.org/10.1021/acsomega.0c01356
ACS Omega 2020, 5, 13963−13972

substrate. The well-visible oscillations of the SERS spectra intensity come from the applied method of measurements. The spectra were recorded point by point along the lines; see Figure 6. Therefore, some correlation between various sections of the measured dependences may occur. The results obtained indicate much greater SERS activity of the layer of Ag nanoparticles deposited on the TiO_2 nanotubes than that deposited on the surface of Ti (as can be seen in Figure 6, the difference in SERS activity is about 1 order of magnitude). In our opinion, it is due to the fact that the "strong SERS signal" is usually associated with a large population of agglomerates of plasmonic nanostructures, and the porous structure of used substrates facilitates the formation of such agglomerates of cubic silver nanoparticles. Moreover, the reproducibility of the substrates was calculated using standard deviation (SD) and relative standard deviation (RSD) from the intensity of the 1004 cm^{-1} band. For the Ti substrate, 114 counts/s (51%), for TiO_2 flat, 9 counts/s (25%), and for TiO_2 NT, 503 counts/s (33%). The smallest RSD was observed for TiO_2 flat, but the average signal value for this medium was the smallest at 37 counts/s. For the TiO_2 NT substrate, the average signal value was 1537 counts/s, while for Ti, which has the highest RSD value (51%), the average signal value was 223 counts/s. The RSD value in relation to the spectrum intensity was the best for the TiO_2 NT substrate. Generally, the repeatability of the measured SERS spectra for nanoporous substrates did not exceed 10% of the RSD value. Despite this, the estimated enhancement factor for TiO_2 NTs was equal to 3.7×10^6, which we have shown in our earlier work.[48,49] Considering the RSD data for flat surfaces, the E_F factor was 2.6×10^5 for Si, 2.8×10^5 for Ti, and 9.1×10^4 for TiO_2 flat, respectively. These differences are due to the reduction of the CR effect and a more even distribution of Ag nanoparticles after wet deposition on a nanoporous substrate. Some statistics data obtained on the basis of SEM image analysis showed also that the amount of Ag CNPs at the central part of the SERS platforms changed from 46 for TiO_2 NTs to 22 for the TiO_2 flat surface, taking into account the same area of analysis of 1 μm^2. It is the result of nanoparticles anchoring by nanotubes and gaps between them. Thus, a specific distribution of nanoparticles onto TiO_2 NTs guarantees the reproducibility of the proposed SERS substrates in contrast to flat substrates where accumulation of nanoparticles at the border was observed.

The TiO_2 NT substrate has a more homogeneous surface coverage with nanoparticles forming "hot spots", which effectively generates the SERS signal. Usually, SERS "hot spots" are observed on sharp structures on surfaces of plasmonic objects (such as sharp apexes and edges) or in slits between plasmonic nanostructures,[50] which takes place in our case. The morphology of the substrate made of TiO_2 NT promotes the retention of nanoparticles between and within the nanotubes. This leads to a fairly repeatable coverage of the substrate, which is visible as a relatively high average signal value. In the case of the TiO_2 flat substrate, the nanoparticles form agglomerates much more often, although the population of nanoparticles that are not in agglomerates is also large. This causes the intensity of the measured SERS spectrum to change significantly because, in agglomerates, SERS "hot spots" can be expected to significantly increase the value of the intensity of the spectra, and in areas where there are single nanoparticles, this signal will be much smaller. The number of agglomerates was lower on Ti than on TiO_2 flat substrates. The ability to form agglomerates in a drying drop may depend on the hydrophobicity of the substrate. If the substrate is more hydrophobic, the number of agglomerates is higher than in the case of a more hydrophilic substrate, although such observations should be confirmed by further research. In addition, the intensity of the SERS spectrum generated using the TiO_2 NT substrate was an average of 2 orders of magnitude larger than when the TiO_2 flat substrate was used. The intensity of the SERS spectra measured using the TiO_2 NT and Ti substrates differed by approximately 1 order of magnitude. This observation can be explained by there being more SERS "hot spots" on the TiO_2 NT surface or also by the fact that few nanoparticles on the TiO_2 NT substrate form a coffee ring. In this situation, there are more nanoparticles in the center of the sample, and the intensity of the SERS signal depends on the amount of nanoparticles that amplify the SERS signal.

CONCLUSIONS

Various titanium substrates (unmodified and modified with a TiO_2 flat layer and a layer of TiO_2 nanotubes) were used as substrates on which layers of cubic silver nanoparticles were deposited. The deposition of silver nanoparticles was carried out by depositing a suspension of nanoparticles and evaporating the solvent. The "coffee ring effect" was significantly smaller on the substrate made of TiO_2 nanotubes as demonstrated through SEM and AES measurements. The deposition of Ag nanoparticles on the other substrates led to the formation of a border layer significantly enriched with silver nanoparticles and having a width of approximately 40 times larger than that of the TiO_2 NT. In addition, the SERS measurements indicated a much larger ratio of the average signal value to the relative standard deviation. The medium with the smallest relative standard deviation was the TiO_2 flat, but the average signal value for the 1004 cm^{-1} peak was only 37 counts/s. The pure titanium substrate was characterized by medium intensity (223 counts/s) and the largest relative standard deviation (51%). In the case of the TiO_2 NT substrate, the average signal value was significantly higher (1537 to 223 counts/s) than that of Ti, whereas the RSD substrate was only 8% larger than that of TiO_2 flat (33 to 25%).

In the case of titanium oxide nanotubes, not only that the inside of the nanotubes themselves acts as capillaries,[34] but also, the spaces between the nanotubes can be treated as spaces between nanopillars.[27,32] This structure of the substrate reduces flow toward the edge of the droplet, thereby reducing the transport of nanoparticles there. In addition, the capillary effects that cause penetration of the nanotubes also cause the penetration of nanoparticles into the spaces inside and outside the nanotubes. The nanoparticles deposited on such a substrate create a very small coffee ring effect, although the substrate itself is superhydrophilic, and on hydrophobic titanium oxide without nanotubes, the CR effect is much greater.

MATERIALS AND METHODS

Materials Used for Research. The following chemical reagents were used to prepare the silver cubic nanoparticles and SERS substrates: trisodium citrate dihydrate, silver nitrate, potassium chloride, ethylene glycol, ethanol, acetone (all of the above reagents were from POCH S.A.), sodium sulfide (Sigma-

https://dx.doi.org/10.1021/acsomega.0c01356
ACS Omega 2020, 5, 13963−13972

Aldrich), polyvinylpyrrolidone (PVP) with an average molar mass of ca. 4×10^4 g/mol (Fluka), glycerin (Chempur), ammonium fluoride (Chempur), and pyridine (UniChem). All of the chemicals were used without further purification or treatment. The water was purified by a Millipore Milli-Q system and had a resistivity of ca. 18 MΩ/cm[11]. A titanium foil (0.25 mm-thick and 99.5% purity) from Alfa Aesar was used to form the ATO (anodic titanium oxide) layer, and the reference was a flat SERS substrate cut into 1 cm^2 round plates. Before anodization, all the plates were cleaned ultrasonically with acetone and ethanol, rinsed with water, and dried in air.

Preparation of the Silver Cubic Nanoparticles. The silver cubic nanoparticles (Ag CNPs) were prepared using the protocol described by Skrabalak et al.[43] with modifications. A volume of 60 mL of ethylene glycol was heated to 170 °C and left for 1 h in a system with a reflux condenser and magnetic stirrer. All the reagent solutions described below were prepared in ethylene glycol. A volume of 1 mL of a 1 mM Na_2S solution and 15 mL of a 180 mM PVP solution (relative to the monomer) were added. After the temperature again reached 170 °C, 5 mL of a 280 mM $AgNO_3$ solution was added. After the color changed to dark green, the solution was quickly cooled in an ice bath. A volume of 1 mL of the nanoparticles obtained was transferred to a centrifuge tube, 9 mL of acetone was added, and the mixture was centrifuged for 5 min. The supernatant was removed, and the nanoparticles were suspended in 10 mL of water and centrifuged again for 3 min. Centrifugation with water was repeated twice.

Preparation of the SERS Substrates. The titanium(IV) oxide nanotubes (TiO_2 NTs) were formed electrochemically by the anodic oxidation of Ti foil in an electrolyte based in water (225 mL), glycerol (225 mL), and ammonium fluoride (4.5 g). The synthesis of the TiO_2 NTs was carried out in a two-electrode cell where the Ti foil was used as the anode. A one-step anodization at a constant voltage of 25 V for 2 h at room temperature was applied. The samples thus prepared were then rinsed and then left in water for 24 h to remove any residual electrolyte. In order to convert the TiO_2 NTs from an amorphous form in the as-received state into the anatase phase, the samples were annealed for 2 h at 450 ° C in air. A flat layer of titanium(IV) oxide (TiO_2 flat) on the titanium foil was achieved by heat treatment under the same conditions as for the TiO_2 NTs. In order to prepare a rough silver electrode (Ag ref.), a pressed silver wire (purchased from the Polish Mint) was used. The working electrode of a silver wire, platinum counter electrode, and reference Ag/AgCl electrode was inserted into the electrolyte solution (0.1 M KCl). Five oxidation−reduction cycles from −300 to 300 mV were carried out with a sweep speed of 5 mV/s. Then, the silver electrode was held for 30 s at −300 mV. After roughing, the electrode was rinsed with water. As a reference material, a Si wafer (Sigma Aldrich) with an area of approximately 1 cm^2 was also used without any functionalization of the surface.

Deposition of the Silver Cubic Nanoparticles on the Substrates. A volume of 200 μL of the Ag CNPs suspension was dropped onto Ti, TiO_2 flat, Si, and TiO_2 NT surfaces and allowed to dry overnight. The resulting substrates were used without any further preparation.

Characterization of the Nanostructures Obtained. An SEM microscope (FEI Nova NanoSEM 450) was used for the morphological characterization of the samples after their anodization, heat treatment, and Ag CNPs functionalization. The examinations were carried out using a through-the-lens detector (TLD) of secondary electrons at a primary beam energy of 10 kV under high vacuum (pressure of 10^{-6} mbar). SEM images were obtained at a long scan acquisition time of, typically, 30 s/frame after the inspection region was chosen. In order to determine approximately the degree of surface coverage of substrates by silver nanoparticles, SEM images from the center and border of the samples presented in the publication were analyzed. The occurrence of nanoparticles in the visible area was counted and then divided by the surface of the sample visible in the image. The approximate amount of nanoparticles per 1 μm^2 was obtained. For the boundary, the amount of the nanoparticles estimated per unit area was multiplied by the CR boundary width for individual substrates.

Contact Angle Measurements. The wetting properties of the surface of the samples were characterized by their (static) water contact angle (WCA). Measurements were made using the sessile drop method using a manual optical tensiometer (Theta Lite, Attension). A drop of distilled water (5 μL) was placed at the surface of the samples using a microsyringe. The contact angles within 1 s were monitored, and the average of at least three measurements was calculated.

SERS Measurements. Raman measurements were carried out using a Jobin-Yvon Labram HR800 spectrometer equipped with a 600-groove/mm holographic grating, a Peltier-cooled CCD detector (1024 × 256 pixels), and an Olympus BX40 microscope with a long distance 50× objective. The numerical aperture is equal to 0.5. A Nd:YAG laser (532 nm) was used in all measurements. The laser power at the sample is approximately 1 mW. A solution of 50 mM pyridine in 0.1 M KCl was used as the probe molecule for the SERS investigations. A volume of 200 μL of the pyridine solution was deposited onto the prepared substrates, and then the SERS spectra were recorded before the drop dried. It should be noted here that, after the drop of the pyridine solution has dried, the intensity of the measured SERS signal is very irreproducible since the formed small crystals of salt disturb the path of the incident and the scattered light. Thus, the SERS measurements were carried out only for substrates covered with the layer of pyridine solution. The laser spot size was approximately 1 μm^2.

Pyridine spectra were performed for all of the substrates, the electrochemically roughened silver electrode, and the nanoparticles. The 400 spectra in an area of 60 × 60 microns were taken and averaged. For all of these measurements, the acquisition time of a single spectrum was 1 s. These spectra were taken also to compare the background.

AES Measurements. High-resolution scanning Auger microprobe-microlab 350 (Thermo Electron) equipped with an FEG-tip (field-emission electron gun, Schottky source) was used for AES analysis. The spectrometer was used to visualize the morphology and determine the chemical composition in the coffee ring-effect area. Detailed lateral distributions of the elements Ti LMM, O KLL, C KLL, and Ag MNN were examined at the interface between the drop and the substrate (TiO_2 NT, TiO_2 flat, and Ti plate). Taking into account the differences in the atomic mass (Z) of the investigated elements C, O, Ti, and Ag, the best ratio of the intensity signal of individual elements was obtained for C and Ag with background correction. Therefore, for C KLL and Ag MNN signals, linear profiles were determined. Auger spectra were recorded at E = 10 kV in steps of kinetic energy of 1.0 eV. Avantage software (ver. 4.88) was used for data processing.

https://dx.doi.org/10.1021/acsomega.0c01356
ACS Omega 2020, 5, 13963−13972

AUTHOR INFORMATION

Corresponding Author

Marcin Pisarek − *Institute of Physical Chemistry, Polish Academy of Sciences, Laboratory of Surface Analysis, 01-224 Warsaw, Poland;* orcid.org/0000-0002-7424-5954; Email: mpisarek@ichf.edu.pl

Authors

Robert Ambroziak − *Faculty of Chemistry, University of Warsaw, 02-093 Warsaw, Poland*

Jan Krajczewski − *Faculty of Chemistry, University of Warsaw, 02-093 Warsaw, Poland*

Andrzej Kudelski − *Faculty of Chemistry, University of Warsaw, 02-093 Warsaw, Poland;* orcid.org/0000-0003-1452-5951

Complete contact information is available at: https://pubs.acs.org/10.1021/acsomega.0c01356

Notes

The authors declare no competing financial interest.

ACKNOWLEDGMENTS

This work was financially supported by the Laboratory of Surface Analysis (Institute of Physical Chemistry PAS) and Faculty of Chemistry, University of Warsaw.

REFERENCES

(1) Fang, W.; Jia, S.; Chao, J.; Wang, L.; Duan, X.; Liu, H.; Li, Q.; Zuo, X.; Wang, L.; Wang, L.; et al. Quantizing single-molecule surface-enhanced Raman scattering with DNA origami metamolecules. *Sci. Adv.* **2019**, *5*, No. eaau4506.

(2) Etchegoin, P. G.; Le Ru, E. C. A perspective on single molecule SERS: Current status and future challenges. *Phys. Chem. Chem. Phys.* **2008**, *10*, 6079−6089.

(3) Marshall, A. R. L.; Stokes, J.; Viscomi, F. N.; Proctor, J. E.; Gierschner, J.; Bouillard, J.-S. G.; Adawi, A. M. Determining molecular orientation: Via single molecule SERS in a plasmonic nano-gap. *Nanoscale* **2017**, *9*, 17415−17421.

(4) Hoppmann, E. P.; Yu, W. W.; White, I. M. Highly sensitive and flexible inkjet printed SERS sensors on paper. *Methods* **2013**, *63*, 219−224.

(5) Yu, W. W.; White, I. M. Inkjet-printed paper-based SERS dipsticks and swabs for trace chemical detection. *Analyst* **2013**, *138*, 1020−1025.

(6) Micciché, C.; Arrabito, G.; Amato, F.; Buscarino, G.; Agnello, S.; Pignataro, B. Inkjet printing Ag nanoparticles for SERS hot spots. *Anal. Methods* **2018**, *10*, 3215−3223.

(7) Li, D.; Cao, X.; Zhang, Q.; Ren, X.; Jiang, L.; Li, D.; Deng, W.; Liu, H. Facile: In situ synthesis of core-shell MOF@Ag nanoparticle composites on screen-printed electrodes for ultrasensitive SERS detection of polycyclic aromatic hydrocarbons. *J. Mater. Chem. A* **2019**, *7*, 14108−14117.

(8) Dustov, M.; Golovina, D. I.; Polyakov, A. Y.; Goldt, A. E.; Eliseev, A. A.; Kolesnikov, E. A.; Sukhorukova, I. V.; Shtansky, D. V.; Grünert, W.; Grigorieva, A. V. Silver eco-solvent ink for reactive printing of polychromatic SERS and SPR substrates. *Sensors* **2018**, *18*, 521.

(9) Cailletaud, J.; De Bleye, C.; Dumont, E.; Sacré, P.-Y.; Gut, Y.; Bultel, L.; Ginot, Y.-M.; Hubert, P.; Ziemons, E. Towards a spray-coating method for the detection of low-dose compounds in pharmaceutical tablets using surface-enhanced Raman chemical imaging (SER-CI). *Talanta* **2018**, *188*, 584−592.

(10) López-Lorente, A. I.; Picca, R. A.; Izquierdo, J.; Kranz, C.; Mizaikoff, B.; Di Franco, C.; Cárdenas, S.; Cioffi, N.; Palazzo, G.; Valentini, A. Ion beam sputtering deposition of silver nanoparticles and TiOx/ZnO nanocomposites for use in surface enhanced vibrational spectroscopy (SERS and SEIRAS). *Microchim. Acta* **2018**, *185*, 153.

(11) Kouba, K.; Proška, J.; Procházka, M. Gold film over SiO2 nanospheres—new thermally resistant substrates for surface-enhanced Raman scattering (SERS) spectroscopy. *Nanomaterials* **2019**, *9*, 1426.

(12) Gupta, S.; Agrawal, M.; Conrad, M.; Hutter, N. A.; Olk, P.; Simon, F.; Eng, L. M.; Stamm, M.; Jordan, R. Poly(2-(dimethylamino)ethyl methacrylate) brushes with incorporated nanoparticles as a SERS active sensing layer. *Adv. Funct. Mater.* **2010**, *20*, 1756−1761.

(13) Ou, Y.; Wang, L.-Y.; Zhu, L.-W.; Wan, L.-S.; Xu, Z.-K. In-situ immobilization of silver nanoparticles on self-assembled honeycomb-patterned films enables surface-enhanced raman scattering (SERS) substrates. *J. Phys. Chem. C* **2014**, *118*, 11478−11484.

(14) Liu, J.; Si, T.; Zhang, Z. Mussel-inspired immobilization of silver nanoparticles toward sponge for rapid swabbing extraction and SERS detection of trace inorganic explosives. *Talanta* **2019**, *204*, 189−197.

(15) Caro, C.; Gámez, F.; Zaderenko, A. P. Preparation of surface-enhanced raman scattering substrates based on immobilized silver-capped nanoparticles. *J. Spectrosc.* **2018**, *2018*, 4127108.

(16) Hutter, E.; Fendler, J. H.; Roy, D. Surface plasmon resonance studies of gold and silver nanoparticles linked to gold and silver substrates by 2-aminoethanethiol and 1,6-hexanedithiol. *J. Phys. Chem. B* **2001**, *105*, 11159−11168.

(17) Kariuki, N. N.; Luo, J.; Hassan, S. A.; Lim, I.-I. S.; Wang, L.; Zhong, C. J. Assembly of bimetallic gold-silver nanoparticles via selective interparticle dicarboxylate-silver linkages. *Chem. Mater.* **2006**, *18*, 123−132.

(18) Mampallil, D.; Eral, H. B. A review on suppression and utilization of the coffee-ring effect. *Adv. Colloid Interface Sci.* **2018**, *252*, 38−54.

(19) Deegan, R. D.; Bakajin, O.; Dupont, T. F.; Huber, G.; Nagel, S. R.; Witten, T. A. Capillary flow as the cause of ring stains from dried liquid drops. *Nature* **1997**, *389*, 827−829.

(20) Chen, R.; Zhang, L.; Li, X.; Ong, L.; Soe, Y. G.; Sinsua, N.; Gras, S. L.; Tabor, R. F.; Wang, X.; Shen, W. Trace analysis and chemical identification on cellulose nanofibers-textured SERS substrates using the "coffee ring" effect. *ACS Sens.* **2017**, *2*, 1060−1067.

(21) Wang, W.; Yin, Y.; Tan, Z.; Liu, J. Coffee-ring effect-based simultaneous SERS substrate fabrication and analyte enrichment for trace analysis. *Nanoscale* **2014**, *6*, 9588−9593.

(22) Semenova, A. A.; Goodilin, E. A.; Brazhe, N. A.; Ivanov, V. K.; Baranchikov, A. E.; Lebedev, V. A.; Goldt, A. E.; Sosnovtseva, O. V.; Savilov, S. V.; Egorov, A. V.; et al. Planar SERS nanostructures with stochastic silver ring morphology for biosensor chips. *J. Mater. Chem.* **2012**, *22*, 24530−24544.

(23) Keskin, S.; Çulha, M. Label-free detection of proteins from dried-suspended droplets using surface enhanced Raman scattering. *Analyst* **2012**, *137*, 2651−2657.

(24) Wang, H.; Fang, J.; Xu, J.; Wang, F.; Sun, B.; He, S.; Sun, G.; Liu, H. A hanging plasmonic droplet: Three-dimensional SERS hotspots for a highly sensitive multiplex detection of amino acids. *Analyst* **2015**, *140*, 2973−2978.

(25) Yang, Q.; Deng, M.; Li, H.; Li, M.; Zhang, C.; Shen, W.; Li, Y.; Guo, D.; Song, Y. Highly reproducible SERS arrays directly written by inkjet printing. *Nanoscale* **2015**, *7*, 421−425.

(26) Kołątaj, K.; Ambroziak, R.; Kędziora, M.; Krajczewski, J.; Kudelski, A. Formation of bifunctional conglomerates composed of magnetic γ-Fe_2O_3 nanoparticles and various noble metal nanostructures. *Appl. Surf. Sci.* **2019**, *470*, 970−978.

(27) Semprebon, C.; Forsberg, P.; Priest, C.; Brinkmann, M. Pinning and wicking in regular pillar arrays. *Soft Matter* **2014**, *10*, 5739−5748.

(28) Dash, S.; Garimella, S. V. Droplet evaporation dynamics on a superhydrophobic surface with negligible hysteresis. *Langmuir* **2013**, *29*, 10785−10795.

(29) He, A.; Yang, H.; Xue, W.; Sun, K.; Cao, Y. Tunable coffee-ring effect on a superhydrophobic surface. *Opt. Lett.* **2017**, *42*, 3936.

(30) Anyfantakis, M.; Baigl, D. Manipulating the Coffee-Ring Effect: Interactions at Work. *ChemPhysChem* **2015**, *16*, 2726−2734.
(31) Nguyen, T. A. H.; Hampton, M. A.; Nguyen, A. V. Evaporation of nanoparticle droplets on smooth hydrophobic surfaces: The inner coffee ring deposits. *J. Phys. Chem. C* **2013**, *117*, 4707−4716.
(32) Cui, L.; Zhang, J.; Zhang, X.; Li, Y.; Wang, Z.; Gao, H.; Wang, T.; Zhu, S.; Yu, H.; Yang, B. Avoiding coffee ring structure based on hydrophobic silicon pillar arrays during single-drop evaporation. *Soft Matter* **2012**, *8*, 10448−10456.
(33) Pack, M.; Hu, H.; Kim, D.-O.; Yang, X.; Sun, Y. Colloidal Drop Deposition on Porous Substrates: Competition among Particle Motion, Evaporation, and Infiltration. *Langmuir* **2015**, *31*, 7953−7961.
(34) Liu, G.; Du, K.; Wang, K. Surface wettability of TiO 2 nanotube arrays prepared by electrochemical anodization. *Appl. Surf. Sci.* **2016**, *388*, 313−320.
(35) Andrzejczuk, M.; Roguska, A.; Pisarek, M.; Hołdyński, M.; Lewandowska, M.; Kurzydłowski, K. J. Morphology of TiO2 nanotubes revealed through electron tomography. *Micron* **2017**, *95*, 35−41.
(36) Roguska, A.; Pisarek, M.; Belcarz, A.; Marcon, L.; Holdynski, M.; Andrzejczuk, M.; Janik-Czachor, M. Improvement of the bio-functional properties of TiO_2 nanotubes. *Appl. Surf. Sci.* **2016**, *388*, 775−785.
(37) Wang, R.; Sakai, N.; Fujishima, A.; Watanabe, T.; Hashimoto, K. Studies of surface wettability conversion on TiO_2 single-crystal surfaces. *J. Phys. Chem. B* **1999**, *103*, 2188−2194.
(38) Kissinger, G.; Kissinger, W. Hydrophilicity of Silicon Wafers for Direct Bonding. *Phys. Status Solidi* **1991**, *123*, 185−192.
(39) Feng, A.; McCoy, B. J.; Munir, Z. A.; Cagliostro, D. Wettability of transition metal oxide surfaces. *Mater. Sci. Eng., A* **1998**, *242*, 50−56.
(40) Yunker, P. J.; Still, T.; Lohr, M. A.; Yodh, A. G. Suppression of the coffee-ring effect by shape-dependent capillary interactions. *Nature* **2011**, *476*, 308−311.
(41) Hao, E.; Schatz, G. C. Electromagnetic fields around silver nanoparticles and dimers. *J. Chem. Phys.* **2004**, *120*, 357−366.
(42) Pisarek, M.; Roguska, A.; Kudelski, A.; Andrzejczuk, M.; Janik-Czachor, M.; Kurzydłowski, K. J. The role of Ag particles deposited on TiO_2 or Al_2O_3 self-organized nanoporous layers in their behavior as SERS-active and biomedical substrates. *Mater. Chem. Phys.* **2013**, *139*, 55−65.
(43) Skrabalak, S. E.; Au, L.; Li, X.; Xia, Y. Facile synthesis of Ag nanocubes and Au nanocages. *Nat. Protoc.* **2007**, *2*, 2182−2190.
(44) Zuo, C.; Jagodzinski, P. W. Surface-enhanced raman scattering of pyridine using different metals: Differences and explanation based on the selective formation of α-pyridyl on metal surfaces. *J. Phys. Chem. B* **2005**, *109*, 1788−1793.
(45) Kudelski, A.; Pettinger, B. SERS on carbon chain segments: Monitoring locally surface chemistry. *Chem. Phys. Lett.* **2000**, *321*, 356−362.
(46) Xia, X.; Zeng, J.; Oetjen, L. K.; Li, Q.; Xia, Y. Quantitative analysis of the role played by poly(vinylpyrrolidone) in seed-mediated growth of Ag nanocrystals. *J. Am. Chem. Soc.* **2012**, *134*, 1793−1801.
(47) Alessio, P.; Constantino, C. J. L.; Aroca, R. F.; Oliveira, O. N., Jr. Surface-enhanced raman scattering: Metal nanostructures coated with langmuir-blodgett films. *J. Chil. Chem. Soc.* **2010**, *55*, 469−478.
(48) Ambroziak, R.; Hołdyński, M.; Płociński, T.; Pisarek, M.; Kudelski, A. Cubic silver nanoparticles fixed on TiO_2 nanotubes as simple and efficient substrates for surface enhanced Raman scattering. *Materials* **2019**, *12*, 3373.
(49) Pisarek, M.; Holdynski, M.; Roguska, A.; Kudelski, A.; Janik-Czachor, M. TiO_2 and Al_2O_3 nanoporous oxide layers decorated with silver nanoparticles—active substrates for SERS measurements. *J. Solid State Electrochem.* **2014**, *18*, 3099−3109.
(50) Kneipp, K.; Wang, Y.; Dasari, R. R.; Feld, M. S. Approach to Single Molecule Detection Using Surface-Enhanced Resonance Raman Scattering (SERRS): A Study Using Rhodamine 6G on Colloidal Silver. *Appl. Spectrosc.* **1995**, *49*, 780−784.

https://dx.doi.org/10.1021/acsomega.0c01356
ACS Omega 2020, 5, 13963−13972